A Modified Deadbeat Predictive Current Control for Improving Dynamic Performance of PMSM

Zixuan Liu, Xiaoyan Huang, *Member, IEEE*, Qichao Hu, Zhaokai Li, *Member, IEEE*, Ze Jiang, Yelong Yu, and Zhuo Chen

***Abstract*— This article proposes a modified deadbeat predictive current control (M-DPCC) method to improve the dynamic performance of permanent magnet synchronous motor (PMSM). Classical DPCC only predicts one control cycle of the PMSM, which restricts the dynamic performance since multiple control cycles are required for the transient state under heavy load and rated speed working condition. The proposed M-DPCC extends the single-step prediction to the entire dynamic interval in the transient state, by which the comprehensive optimization on the angle of the stator voltage vector can be implemented. Moreover, M-DPCC performed multi-step deadbeat calculation to keep the computation modest. To verify the effectiveness of the proposed M-DPCC, transient-state performance of PMSM using the M-DPCC method, the modulated model predictive control and classical DPCC are explored under a wide range of working condition. Comparative simulation and experimental results indicate that dynamic performance of the PMSM can be improved, especially under rated speed and heavy load conditions. Besides, the parameter sensitivity to inductance mismatch of the three methods is carried out. The stable operation range of the M-DPCC under inductance mismatch is larger than the other two methods. Moreover, the computation complexity of the three methods were investigated. The M-DPCC acquired less computation time than the modulated model predictive control.**

***Index Terms*—Deadbeat predictive current control (DPCC), dynamic performance, permanent-magnet synchronous motor (PMSM), prediction horizon, transient-state operation.**

I. Introduction

PERMANENT-magnet synchronous machines (PMSMs) draw worldwide attention in decades of research owing to their high power density and high efficiency [1]. Among various control strategies for inverter-fed PMSM, model predictive current control (MPCC) shows promising performance due to its simple principle and great performance [2]–[3]. Most MPCC methods aim to eliminate the errors of stator currents using the optimal voltage vector (VV). Basically, three classes of methods are used to enhance the dynamic performance, decrease the steady-state torque ripple, and reduce the computation complexity [4]–[36].

The first class is finite control set MPCC [4], which makes predictions of the future states of PMSM fed by every possible VV from the inverter. When applying longer prediction horizon, the performance of PMSM can be significantly improved [5], but it is greatly limited by the computational ability of the microcontroller. Hence, many efforts have been made to decrease the computation burden. Cagienard *et al.* [6] employed two parts of prediction horizon with different prediction resolution. In [7], the extrapolation strategy was introduced to extend the prediction horizon until the extrapolated trajectories of the control objectives reach their hysteresis bounds. In [8], Jlassi and Cardoso make classification of all possible VVs using novel lookup table to decrease the number of VVs in the evaluation. Instead of increasing the prediction horizon, the second class extends the possible VVs. Therefore, a more proper VV can be selected. Petkar *et al.* [9] applied an active VV and a zero VV to MPCC in one control cycle for reducing torque ripple. Furthermore, the number of active VVs was increased to enhance the dynamic performance of PMSM [10]. The same method in [10] was introduced to reduce the torque ripple [11] and flux ripple [12] in the steady state. However, these methods in [6]–[12] still faced increasing calculation burden when the prediction horizon and the number of VVs extended.

To avoid such problem, the third class of MPCC, i.e., deadbeat predictive current control (DPCC), is introduced to directly obtain the optimal VV using the explicit evaluation method. The errors of the control objectives are eliminated in one control cycle [4]. The research about DPCC mainly focused on parameter mismatch [13]–[14], fault tolerant [15], lower computation burden [16], and current harmonic reduction [17], [18]. In [19]–[21], discrete space vector modulation was introduced to modulate the optimal VV of DPCC in fixed switching frequency. Only a small group of VVs were selected to decrease the computation amount. Besides, classical space vector pulsewidth modulation (SVM) was introduced to obtain the amplitude and the angle of the optimal VV [22]–[25]. However, when the back electromagnetic force is close to the limitation of SVM linear modulation

Manuscript received 22 September 2021; revised 4 December 2021, 13 March 2022, and 19 May 2022; accepted 26 June 2022. Date of publication 6 July 2022; date of current version 6 September 2022. This work was supported in part by the National Key R&D Program of China under Grant 2019YFE0123500, in part by the Zhejiang Provincial Ten-Thousand-Talent Plan under Grant 2019R52003, and in part by the Liaoning Provincial Natural Science Foundation of China under Grant 2021-KF-24-03. Recommended for publication by Associate Editor R. Kennel. *(Corresponding authors: Zhaokai Li; Xiaoyan Huang.)*

Zixuan Liu, Xiaoyan Huang, Qichao Hu, Zhaokai Li, Yelong Yu, and Zhuo Chen are with the Zhejiang Provincial Key Laboratory of Electrical Machine Systems, College of Electrical Engineering, Zhejiang University, Hangzhou 310027, China (e-mail: eelzx@zju.edu.cn; xiaoyanhuang@zju.edu.cn; eehqc@zju.edu.cn; lzk_zju@zju.edu.cn; yueylong@zju.edu.cn; z.chen@zju.edu.cn).

Ze Jiang is with the College of Electrical Engineering, Zhejiang University, Hangzhou 310027, China, and also with the Wolong Electric Group Co., Ltd, Shaoxing 312300, China (e-mail: jiangze@wolong.com).

Color versions of one or more figures in this article are available at https://doi.org/10.1109/TPEL.2022.3188761.

Digital Object Identifier 10.1109/TPEL.2022.3188761

region, or when the current drop on the stator resistance becomes unignorable, there is lack of voltage to produce stator current and degrade the dynamic performance. In another word, when the PMSM is operated under rated speed and heavy load condition, the optimal VV from DPCC will outrange the linear region of SVM in the dynamic process [26]–[28]. Most DPCC methods reduced the amplitude of the optimal VV. Hence, the modified VV can be subject to the limitations on the voltage actuation [22]–[28]. However, the unpredicted errors of the *dq*-axes currents were introduced in the transient state, reducing the dynamic performance of DPCC. Besides, the influence of the optimal VV distortion is unforeseeable as the DPCC only makes a single-step prediction.

To solve these problems, various methods have been proposed to achieve smooth transition from linear modulation to six-step mode [29]–[36]. Most of them focus on the improvement of the steady-state performance. However, there are few literatures about the over-modulation in the transient state of DPCC. In [35], the modulated model predictive control (MMPC) introduced optimal overmodulation in single-step to have a minimum cost function and improve the dynamic performance, but the computation complexity increased. Then, in [36], the calculation was simplified to reduce the computation complexity, but the optimization in long prediction horizon was neglected due to the heavy computation burden. It is necessary and significant for DPCC to achieve optimal modulation in long prediction horizon while keeping the computation modest.

The main objectives of this article are to design a modified DPCC (M-DPCC) with adaptive prediction horizon and reduced computational complexity to improve the dynamic performance of conventional DPCC. Rather than single-step prediction in the MMPC and conventional DPCC, the horizon is adaptively extended to the entire transient state in M-DPCC. To avoid heavy computation caused by multistep FCS-MPC prediction, the multiple-step deadbeat prediction differential equations were introduced. Then, the special method to reduce the order of the equations and to set the initial value was adopted to keep the computation modest. For parameter sensitivity, the M-DPCC shows stronger robustness against inductance mismatch while the MMPC and classical DPCC shows larger current total harmonic distortion (THD) and steady-state error.

II. PMSM Model and Classical DPCC Method

A. PMSM Model

The electrical dynamics of PMSM in *dq*-axes can be given by

$$\boldsymbol{u}_{dq} = p\boldsymbol{\psi}_{sdq} + \omega_e \begin{bmatrix} 0 & -1 \\ 1 & 0 \end{bmatrix} \boldsymbol{\psi}_{sdq} + \boldsymbol{R}_s \boldsymbol{i}_{dq} \tag{1}$$

$$\boldsymbol{\psi}_{sdq} = \boldsymbol{L}_{dq} \boldsymbol{i}_{dq} + \boldsymbol{\psi}_{fdq} \tag{2}$$

where $\boldsymbol{u}_{dq} = [u_d \ u_q]^T$, $\boldsymbol{\psi}_{dq} = [\psi_d \ \psi_q]^T$, $\boldsymbol{i}_{dq} = [i_d \ i_q]^T$ are the VV, stator flux linkage, and stator current in *dq*-axes respectively, and

$$\boldsymbol{L}_{dq} = \begin{bmatrix} L_d & 0 \\ 0 & L_q \end{bmatrix}, \boldsymbol{\psi}_{fdq} = \begin{bmatrix} \psi_f \\ 0 \end{bmatrix}, \boldsymbol{R}_s = \begin{bmatrix} R & 0 \\ 0 & R \end{bmatrix}$$

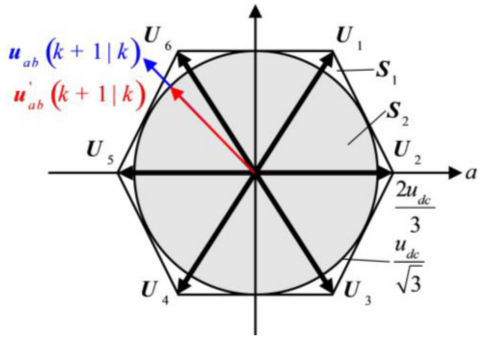

Fig. 1. Classical DPCC modulation method when optimal VV is out of linear modulation region of SVM.

where $L_{d,q}$, ψ_f, and $\boldsymbol{R}$ are the *dq*-axes stator inductance, permanent magnet flux, and stator resistance, respectively. By substituting (2) into (1), and utilizing Euler's method, the discrete model of stator current of PMSM is obtained as

$$\boldsymbol{u}_{dq}(k) = \boldsymbol{A} i_{dq}(k+1) + \boldsymbol{B} i_{dq}(k) + \boldsymbol{C} \tag{3}$$

where

$$\boldsymbol{u}_{dq}(k) = \left[u_d(k) \ u_q(k)\right]^T,$$
$$\boldsymbol{i}_{dq}(k) = \left[i_d(k) \ i_q(k)\right]^T$$

are the VV and current in the kth control cycle in *dq*-axes, respectively, and

$$\boldsymbol{A} = \begin{bmatrix} \frac{L_d}{T_s} & 0 \\ 0 & \frac{L_q}{T_s} \end{bmatrix}, \boldsymbol{B} = \begin{bmatrix} R - \frac{L_d}{T_s} & -\omega_e L_q \\ \omega_e L_d & R - \frac{L_q}{T_s} \end{bmatrix}, \boldsymbol{C} = \begin{bmatrix} 0 \\ \omega_e \psi_f \end{bmatrix}$$

where T_s is the control period.

B. Classical DPCC Principle

In the $(k+1)^{th}$ control cycle, the predicted current $\boldsymbol{i}_{dq}(k+1|k)$ could be derived using (3)

$$\boldsymbol{i}_{dq}(k+1|k) = \boldsymbol{A}^{-1}\left(\boldsymbol{u}_{dq}(k) - \boldsymbol{B} i_{dq}(k) - \boldsymbol{C}\right). \tag{4}$$

For microprocessor based digital control systems, the update of pulsewidth modulation (PWM) module is one control cycle delayed, *i.e.*, the desired VV implemented on the $(k+1)^{th}$ control cycle is updated on the k^{th} control cycle. Hence, one can get by substituting (4) into (3) that

$$\boldsymbol{u}_{dq}(k+1|k) = \boldsymbol{A}\boldsymbol{i}^*_{dq} + \boldsymbol{B}\boldsymbol{i}_{dq}(k+1|k) + \boldsymbol{C} \tag{5}$$

where $\boldsymbol{u}_{dq}(k+1|k)$ is the optimal VV implemented on the $(k+1)^{th}$ control cycle and updated on the k^{th} control cycle. $\boldsymbol{i}^*_{dq}$ is the *dq*-axes current reference.

C. Drawback of Classical DPCC Modulation Method

SVM is used in classical DPCC methods to modulate the implemented VV $\boldsymbol{u}_{dq}(k+1|k)$ in the stationary reference frame as $\boldsymbol{u}_{\alpha\beta}(k+1|k)$. Classical DPCC modulation method is shown in Fig. 1. $\boldsymbol{U}_{1,\ldots 6}$ are the six active VVs of three phase two-level inverters. The amplitude of active VV is $\frac{2u_{dc}}{3}$, where u_{dc} is the

dc-link voltage. $\boldsymbol{S}_1$ is the region of all possible VVs generated by SVM, and $\boldsymbol{S}_2$ is the linear modulation region of SVM, the radium of which is $\frac{u_{\rm dc}}{\sqrt{3}}$. When the speed is close to rated speed and the current variation is large, the optimal VV may be out of $\boldsymbol{S}_2$

$$\boldsymbol{u}_{\alpha\beta}\left(k+1|k\right) \notin \boldsymbol{S}_2. \tag{6}$$

The classical modulation method reduces the amplitude of the optimal VV down to the limitation of linear region while maintaining the vector angle

$$\left\|\boldsymbol{u}'_{\alpha\beta}\left(k+1|k\right)\right\| = \frac{u_{\rm dc}}{\sqrt{3}} \tag{7}$$

$$\angle\boldsymbol{u}'_{\alpha\beta}\left(k+1|k\right) = \angle\boldsymbol{u}_{\alpha\beta}\left(k+1|k\right) \tag{8}$$

where $\angle\boldsymbol{u}'_{\alpha\beta}(k+1|k)$ is the VV implemented instead of optimal VV after the modulation. As shown in Fig. 1, the blue vector and red vector are the optimal VV and the one limited by the linear region, respectively. By substituting (7) and (8) into (4), the current in the $(k+2)^{th}$ control cycle is obtained

$$\boldsymbol{i}_{dq}\left(k+2|k\right) = \boldsymbol{A}^{-1}\begin{pmatrix}\boldsymbol{u}'_{dq}\left(k+1|k\right)\\ -\boldsymbol{B}\boldsymbol{i}_{dq}\left(k+1|k\right)-\boldsymbol{C}\end{pmatrix}. \tag{9}$$

One can get the uneliminated current error in the $(k+2)^{th}$ control cycle from (5) and (9) as

$$\boldsymbol{i}^*_{dq} - \boldsymbol{i}_{dq}\left(k+2|k\right) = \boldsymbol{A}^{-1}\begin{pmatrix}\boldsymbol{u}_{dq}\left(k+1|k\right)\\ -\boldsymbol{u}'_{dq}\left(k+1|k\right)\end{pmatrix}. \tag{10}$$

Equation (10) indicates that the classical modulation method in (7) and (8) not only introduces errors of stator current, but also deteriorates the current dynamic performance.

III. Proposed M-DPCC Strategy

The linear modulation region is determined by the number of phases, voltage levels of the inverter, and dc-link voltage, hence the limitation of VV amplitude in (7) is maintained in M-DPCC. In the situation of (6), the current error cannot be eliminated in the $(k+2)^{th}$ control cycle. However, the angle of VV in (8) can be modified to try to eliminate torque error first and enhance the torque dynamic performance.

A. Prediction Horizon Extension

Rather than the single-step prediction in the classical DPCC method, the prediction horizon in M-DPCC is extended to a time interval of the entire dynamic process $t \in (0, \xi)$, and therefore achieve more comprehensive and optimized performance. In the dynamic interval, if the rotor speed ω_e is constant as shown in Fig. 2, one can get

$$\theta_r\left(t\right) = \omega_e t + \theta_r\left(0\right), t \in (0, \xi) \tag{11}$$

where θ_r is the electrical rotor position. *ed*-axis is aligned with rotor position at the end of the interval. *eq*-axis is 90° ahead of *ed*-axis. The transformation between *dq*-axes and *edeq*-axes

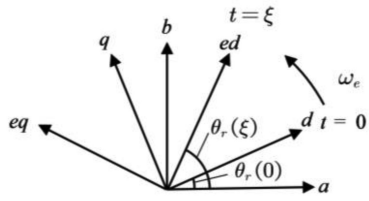

Fig. 2. Rotor position at the end of the dynamic interval.

is obtained

$$\boldsymbol{C}_{dq-edeq} = \begin{bmatrix}\cos\omega_e\left(\xi-t\right) & \sin\omega_e\left(\xi-t\right)\\ -\sin\omega_e\left(\xi-t\right) & \cos\omega_e\left(\xi-t\right)\end{bmatrix} \tag{12}$$

$$\boldsymbol{C}_{edeq-dq} = \boldsymbol{C}^T_{dq-edeq}. \tag{13}$$

By substituting (12) into (1) and (2), one can get the dynamic of PMSM in the proposed stationary *edeq*-axes as

$$\boldsymbol{u}_{edeq} = p\boldsymbol{\psi}_{sedeq} + \boldsymbol{R}_s\boldsymbol{i}_{edeq} \tag{14}$$

where

$$\boldsymbol{u}_{edeq} = \boldsymbol{C}_{dq-edeq}\boldsymbol{u}_{dq}, \boldsymbol{i}_{edeq} = \boldsymbol{C}_{dq-edeq}\boldsymbol{i}_{dq}$$

are the VV and current in *edeq*-axes, respectively, and

$$\begin{aligned}\psi_{sedeq} &= \boldsymbol{C}_{dq-edeq}\psi_{sdq}\\ &= \boldsymbol{L}_{edeq}\boldsymbol{i}_{edeq} + \boldsymbol{C}_{dq-edeq}\psi_{fdq}\end{aligned} \tag{15}$$

is the stator flux linkage in *edeq*-axes, where

$$\boldsymbol{L}_{edeq} = \boldsymbol{C}_{dq-edeq}\boldsymbol{L}_{dq}\boldsymbol{C}^T_{dq-edeq}.$$

One can get the integral of ψ_{sedeq} from (14) in the time interval $t \in (0, \xi)$ as

$$\boldsymbol{\psi}_{sedeq}\big|_0^\xi = \int_0^\xi \boldsymbol{u}_{edeq}dt - \boldsymbol{R}_s\int_0^\xi \boldsymbol{i}_{edeq}dt. \tag{16}$$

Substituting (12), (13) and (15) into (16), one can get

$$\begin{aligned}&\boldsymbol{L}_{dq}\boldsymbol{i}_{edeq}\left(\xi\right) - \boldsymbol{L}_{edeq}\left(0\right)\boldsymbol{i}_{edeq}\left(0\right) + \psi_f\begin{bmatrix}-\cos\left(\omega_e\xi\right)\\ \sin\left(\omega_e\xi\right)\end{bmatrix}\\ &\qquad = \int_0^\xi \boldsymbol{u}_{edeq}dt - \boldsymbol{R}_s\int_0^\xi \boldsymbol{i}_{edeq}dt.\end{aligned} \tag{17}$$

Utilizing Newton–Cotes formula to $\boldsymbol{R}_s\int_0^\xi \boldsymbol{i}_{edeq}dt$ as

$$\boldsymbol{R}_s\int_0^\xi \boldsymbol{i}_{edeq}dt = \boldsymbol{R}_s\xi\frac{\boldsymbol{i}_{edeq}\left(\xi\right)+\boldsymbol{i}_{edeq}\left(0\right)}{2} \tag{18}$$

and substituting (18) into (17), one can get

$$\boldsymbol{i}_{edeq}\left(\xi\right) = \boldsymbol{\sigma}_1^{-1}\int_0^\xi \boldsymbol{u}_{edeq}dt - \boldsymbol{v}_{edeq}\left(\xi\right) \tag{19}$$

where

$$\boldsymbol{v}_{edeq}\left(\xi\right) = \boldsymbol{\sigma}_1^{-1}\left(\psi_f\begin{bmatrix}-\cos\left(\omega_e\xi\right)\\ \sin\left(\omega_e\xi\right)\end{bmatrix} - \boldsymbol{\sigma}_2\boldsymbol{i}_{edeq}\left(0\right)\right)$$

and

$$\boldsymbol{\sigma}_1 = \left(\boldsymbol{L}_{dq} + \frac{\xi}{2}\boldsymbol{R}_s\right), \boldsymbol{\sigma}_2 = \left(\boldsymbol{L}_{edeq}\left(0\right) - \frac{\xi}{2}\boldsymbol{R}_s\right).$$

Equation (19) indicates that the *edeq*-axes current at the end of the interval is only related to the integral of *edeq*-axes VV within the interval and the initial state at the beginning of the interval. Hence, mean value theorem of integrals can be introduced as a simplification to (19)

$$\boldsymbol{i}_{edeq}(\xi) = \boldsymbol{\sigma}_1^{-1}\xi\tilde{\boldsymbol{u}}_{edeq} - \boldsymbol{v}_{edeq}(\xi) \tag{20}$$

where

$$\tilde{\boldsymbol{u}}_{edeq} = \left[\, u_{ed}(\xi_{ed})\ u_{eq}(\xi_{eq}) \,\right]^T, \xi_{ed,eq} \in (0,\xi)$$

and the amplitude limitation of $\tilde{\boldsymbol{u}}_{edeq}$ is given by utilizing Cauchy–Schwarz inequation as

$$\begin{aligned}|\tilde{\boldsymbol{u}}_{edeq}| &\le \frac{1}{\xi}\left(\left(\int_0^\xi u_{ed}(t)\,dt\right)^2 + \left(\int_0^\xi u_{eq}(t)\,dt\right)^2\right)^{\frac{1}{2}} \\ &\le \frac{1}{\sqrt{\xi}}\left(\int_0^\xi \left(u_{ed}(t)^2 + u_{eq}(t)^2\right)dt\right)^{\frac{1}{2}} = u\end{aligned} \tag{21}$$

where $u = \frac{u_{dc}}{\sqrt{3}}$ by substituting limitation (7). Note that the equality of (21) is established if and only if it meets the condition that

$$\boldsymbol{u}_{edeq}(t) \equiv \tilde{\boldsymbol{u}}_{edeq}, t \in (0,\xi). \tag{22}$$

It indicates that the VV within the time interval must maintain constant to reach maximum variation of the stator current. Hence, the current dynamics of PMSM within a flexible time interval can be predicted from (20) rather than (4) for classical DPCC method which only makes a constant single-step prediction.

B. Principle of Multistep Deadbeat Method

To achieve optimal dynamic performance, a multistep deadbeat method is proposed. Within the time interval $t \in (0,\ \xi)$, the torque of the PMSM is given by

$$T_e(t) = \frac{3P}{2}\left(\psi_f i_q(t) + (L_d - L_q)\, i_d(t)\, i_q(t)\right) \tag{23}$$

where P is the number of pole pairs. When $t = \xi$, substituting (12) into (23), one can get the torque in the form of *edeq*-axes current as

$$T_e(\xi) = \frac{3P}{2}\left(\psi_f i_{eq}(\xi) + (L_d - L_q)\, i_{ed}(\xi)\, i_{eq}(\xi)\right). \tag{24}$$

Substituting (20) into (24) one can get

$$T_e(\xi) = k_i \begin{pmatrix} \tau_d\xi\tilde{u}_{ed} \\ -v_{ed}(\xi) \end{pmatrix}\begin{pmatrix} \tau_q\xi\tilde{u}_{eq} \\ -v_{eq}(\xi) \end{pmatrix} + k_p \begin{pmatrix} \tau_q\xi\tilde{u}_{eq} \\ -v_{eq}(\xi) \end{pmatrix} \tag{25}$$

where

$$k_i = \frac{3P(L_d - L_q)}{2L_dL_q}, k_p = \frac{3P\psi_f}{2L_q}$$

$$\tau_d = \frac{2L_d}{2L_d + R\xi}, \tau_q = \frac{2L_d}{2L_d + R\xi}.$$

Assume that the torque reference is written as T_e^*. The torque error is eliminated at the end of the interval when $t = \xi$ as

$$f_1 = T_e(\xi) - T_e^* = 0. \tag{26}$$

To achieve optimal dynamic performance, the torque error must be eliminated first, i.e., should be minimized by introducing Lagrange multiplier method as

$$F = \xi + \lambda\left(\tilde{u}_{ed}^2 + \tilde{u}_{eq}^2 - u^2\right) \tag{27}$$

where limitation in (21) is substituted, F is the Lagrange function and λ is the Lagrange multiplier. To minimize ξ , one can get

$$\begin{cases} \frac{\partial F}{\partial \tilde{u}_{ed}} = \frac{\partial \xi}{\partial \tilde{u}_{ed}} + 2\lambda\tilde{u}_{ed} = 0 \\ \frac{\partial F}{\partial \tilde{u}_{eq}} = \frac{\partial \xi}{\partial \tilde{u}_{eq}} + 2\lambda\tilde{u}_{eq} = 0 \\ \frac{\partial F}{\partial \lambda} = \tilde{u}_{ed}^2 + \tilde{u}_{eq}^2 - u^2 = 0 \end{cases} \tag{28}$$

where

$$\frac{\partial \xi}{\partial \tilde{u}_{ed}} = -\frac{\partial f_1}{\partial \tilde{u}_{ed}}\Big/\frac{\partial f_1}{\partial \xi}, \frac{\partial \xi}{\partial \tilde{u}_{eq}} = -\frac{\partial f_1}{\partial \tilde{u}_{eq}}\Big/\frac{\partial f_1}{\partial \xi}$$

and

$$\frac{\partial f_1}{\partial \tilde{u}_{ed}} = k_i\tau_d\xi\left(\tau_q\xi\tilde{u}_{eq} - v_{eq}(\xi)\right)$$

$$\frac{\partial f_1}{\partial \tilde{u}_{eq}} = k_i\tau_q\xi\left(\tau_d\xi\tilde{u}_{ed} - v_{ed}(\xi)\right) + k_p\tau_q\xi.$$

One can get from (26) and (28) the system of nonlinear equations in the interval as

$$\begin{cases} f_1 = \begin{pmatrix} k_i\left(\tau_d\xi\tilde{u}_{ed} - v_{ed}(\xi)\right)\left(\tau_q\xi\tilde{u}_{eq} - v_{eq}(\xi)\right) \\ +k_p\left(\tau_q\xi\tilde{u}_{eq} - v_{eq}(\xi)\right) \end{pmatrix} \\ -T_e^* = 0 \\ f_2 = \begin{pmatrix} k_i\tau_d\xi\left(\tau_q\xi\tilde{u}_{eq} - v_{eq}(\xi)\right)\tilde{u}_{eq} \\ -k_i\tau_q\xi\left(\tau_d\xi\tilde{u}_{ed} - v_{ed}(\xi)\right)\tilde{u}_{ed} - k_p\tau_q\xi\tilde{u}_{ed} \end{pmatrix} \\ = 0 \\ f_3 = \tilde{u}_{ed}^2 + \tilde{u}_{eq}^2 - u^2 = 0 \end{cases}. \tag{29}$$

Equation (29) indicates that once the torque reference is given, the optimal VV can be solved and the torque error can be eliminated as soon as possible. Newton–Raffson (N–R) algorithm is introduced to directly solve (29). To simplify the calculation, one can get the Jacobi matrix of (29) while the resistor equals zero as

$$\boldsymbol{G}_1 = \begin{bmatrix} \frac{\partial f_1}{\partial \xi} & \frac{\partial f_1}{\partial \tilde{u}_{ed}} & \frac{\partial f_1}{\partial \tilde{u}_{eq}} \\ \frac{\partial f_2}{\partial \xi} & \frac{\partial f_2}{\partial \tilde{u}_{ed}} & \frac{\partial f_2}{\partial \tilde{u}_{eq}} \\ \frac{\partial f_3}{\partial \xi} & \frac{\partial f_3}{\partial \tilde{u}_{ed}} & \frac{\partial f_3}{\partial \tilde{u}_{eq}} \end{bmatrix}. \tag{30}$$

N–R algorithm is obtained as

$$\boldsymbol{x}^{(k+1)} = \boldsymbol{x}^{(k)} - \boldsymbol{G}_1\left(\xi^{(k)}, \tilde{\boldsymbol{u}}_{edeq}^{(k)}\right)^{-1}\boldsymbol{f}\left(\xi^{(k)}, \tilde{\mathbf{u}}_{edeq}^{(k)}\right) \tag{31}$$

where

$$\boldsymbol{x}^{(k)} = \left[\xi^{(k)}\ \tilde{u}_{ed}^{(k)}\ \tilde{u}_{eq}^{(k)}\right]^T, \boldsymbol{f} = \left[\, f_1\ f_2\ f_3 \,\right]^T.$$

For surface-mounted permanent magnet synchronous machine (SPM), (29) can be further simplified to

$$\begin{cases} f_1 = k_p\left(\tau_q\xi\tilde{u}_{eq} - v_{eq}(\xi)\right) - T_e^* = 0 \\ f_2 = -k_p\tau_q\xi\tilde{u}_{ed} = 0 \\ f_3 = \tilde{u}_{ed}^2 + \tilde{u}_{eq}^2 - u^2 = 0 \end{cases} \tag{32}$$

$\tilde{\mathbf{u}}_{edeq}$ can be directly solved as

$$\tilde{u}_{ed}=0,\tilde{u}_{eq}=\begin{cases}u,T_e^*>T_e\left(0\right)\\-u,T_e^*<T_e\left(0\right)\end{cases}. \tag{33}$$

Hence, (31) can also be simplified as

$$\xi^{(k+1)}=\xi^{(k)}-\frac{f_1\left(\xi^{(k)}\right)}{\partial f_1/\partial\xi}. \tag{34}$$

The performance of N–R algorithm is essential to the computation amount of M-DPCC. To enhance the efficiency of N–R algorithm and reduce iterations, the initial value of (34) is chosen as

$$\xi^{(0)}=\begin{cases}\frac{L_q\left(i_q^*-i_q(0)\right)}{u-\omega_e(\psi_f+L_di_d(0))-Ri_q(0)},i_q^*>i_q\left(0\right)\\\frac{L_q\left(i_q^*-i_q(0)\right)}{-u-\omega_e(\psi_f+L_di_d(0))-Ri_q(0)},i_q^*<i_q\left(0\right)\end{cases} \tag{35}$$

where i_q^* is the q-axis current reference.

As the *ed–eq* current vector during multi-step deadbeat process is based on (20) and (33), there exists inter-coupling component in the *ed*-axis. By transforming from *ed–eq* axis to *d–q* axis using (13), the intercoupling component can be observed in d-axis in the transient state.

C. Current Error Elimination Process

When the torque error is eliminated through multistep deadbeat method, the regulation of current error is also required to achieve maximum torque per ampere (MTPA) control. Hence, in the current error elimination process, the amplitude of current vector is reduced while the torque is maintained stable, i.e., the trajectory of current vector must be on the constant torque curve of the PMSM. Assume that the multistep deadbeat process is over

$$T_e\left(k+1|k\right)=T_e^* \tag{36}$$

whereas the current errors are not eliminated. The optimal VV to eliminated the errors is given by (5). When $\boldsymbol{u}_{\alpha\beta}(k+1|k)\in\boldsymbol{S}_2$, the current error can be eliminated in one control cycle. However, when $\boldsymbol{u}_{\alpha\beta}(k+1|k)\notin\boldsymbol{S}_2$ multiple control cycles multiple steps must be considered and torque is maintained constant as

$$\begin{cases}f_4=T_e\left(k+2|k\right)-T_e^*=0\\f_5=u_d(k+1|k)^2+u_q(k+1|k)^2-u^2=0\end{cases}. \tag{37}$$

The Jacobi matrix of (37) is given by

$$\boldsymbol{G}_2=\begin{bmatrix}\frac{\partial f_4}{\partial u_d(k+1|k)}&\frac{\partial f_4}{\partial u_q(k+1|k)}\\\frac{\partial f_5}{\partial u_d(k+1|k)}&\frac{\partial f_5}{\partial u_q(k+1|k)}\end{bmatrix}. \tag{38}$$

N–R algorithm can be implemented as

$$\begin{aligned}&\boldsymbol{u}_{dq}(k+1|k)^{(k+1)}\\&=\begin{pmatrix}\boldsymbol{u}_{dq}(k+1|k)^{(k)}\\-\boldsymbol{G}_2\left(\boldsymbol{u}_{dq}(k+1|k)^{(k)}\right)^{-1}\boldsymbol{h}\left(\boldsymbol{u}_{dq}(k+1|k)^{(k)}\right)\end{pmatrix}\end{aligned} \tag{39}$$

TABLE I
PARAMETERS OF THE TESTED SPM AND DRIVE

Parameter	Value
Stator Resistance	3.5 Ω
Stator Inductance	7.68 mH
Permanent Magnet Flux	0.06165 Wb
Number of Poles	8
Rated Speed	800 r/min
DC-link Voltage	48 V
Control Period	100 uS

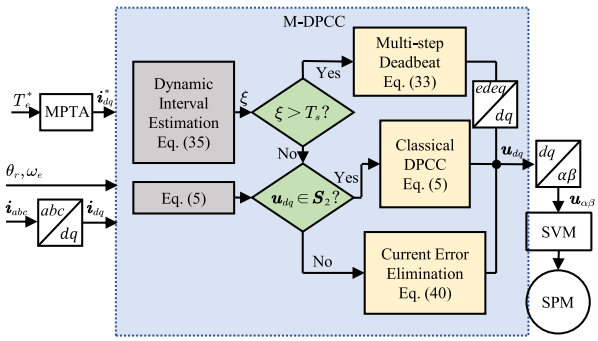

Fig. 3. Diagram of the proposed M-DPCC.

where $\boldsymbol{h}=\left[\,f_4\;f_5\,\right]^T$. For SPM, $\boldsymbol{u}_{dq}(k+1|k)$ can be directly solved from (37) as

$$\begin{cases}u_q\left(k+1|k\right)=R_si_q\left(k+1|k\right)\\+L_d\omega_ei_d\left(k+1|k\right)+\psi_f\omega_e\\u_d\left(k+1|k\right)=\begin{cases}u_d,i_d\left(k+1|k\right)<i_d^*\\-u_d,i_d\left(k+1|k\right)>i_d^*\end{cases}\end{cases} \tag{40}$$

where $u_d=\sqrt{u^2-u_q(k+1|k)^2}$. Equation (40) indicates that in the current error elimination process, when the optimal VV is out of the linear modulation region, only d-axis stator voltage is limited while q-axis voltage is maintained. Thus, in SPM the q-axis current, i.e., the torque maintains stable.

IV. SIMULATION AND EXPERIMENTAL RESULTS

Simulations based on MATLAB/Simulink and experimental results for the torque performance improvement of M-DPCC compared to the classical DPCC are carried out in this section. The SPM motor and its drive parameters are given in Table I. The control diagram of M-DPCC is shown in Fig. 3. The dynamic interval is estimated first. If $\xi>T_s$, it indicates that the dynamic process consists of multiple control period, the multi-step deadbeat method is implemented and the optimal VV of the entire dynamic process is applied to the motor. If $\xi\le T_s$, it means the torque error can be eliminated in one single control cycle, the multistep deadbeat process ends and control objectives change to the elimination of current errors.

When the optimal VV of classical DPCC$u_{dq}\notin S_2$, which means the current error cannot be eliminated in one control cycle, (40) is implemented to stabilize the torque within the current error elimination process. Finally, when $u_{dq}\notin S_2$, which means

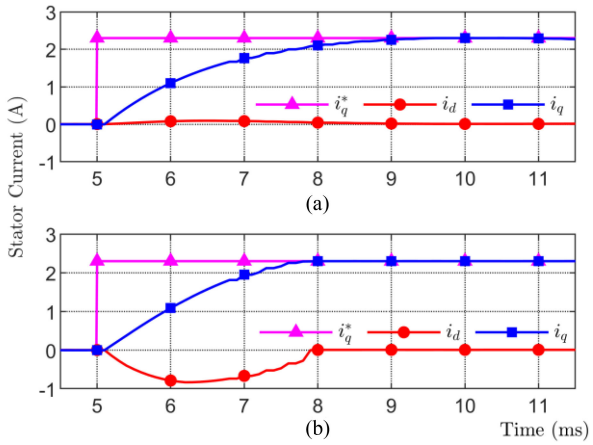

Fig. 4. Simulation results of current dynamic performance at 600 r/min, current reference is 2.3A. (a) Classical DPCC. (b) Modified deadbeat predictive current control.

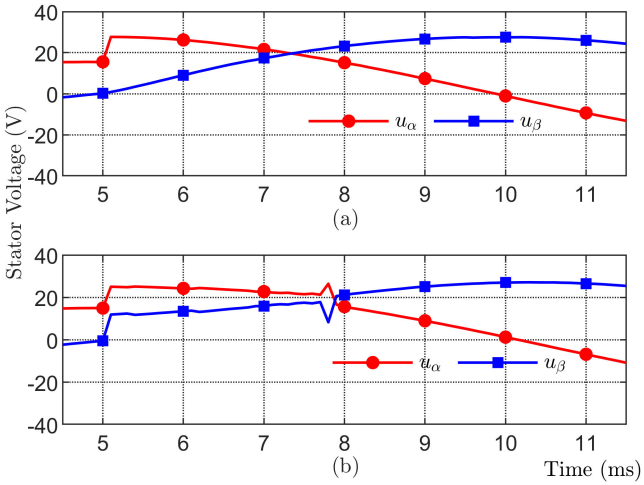

Fig. 5. Simulation results of stator voltage at 600 r/min, current reference is 2.3 A. (a) Classical DPCC. (b) Modified deadbeat predictive current control.

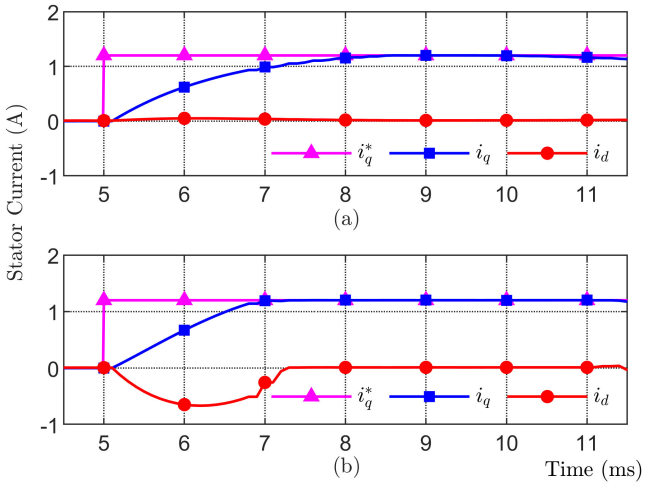

Fig. 6. Simulation results of current dynamic performance at 800 r/min, current reference is 1.2A. (a) Classical DPCC. (b) Modified deadbeat predictive current control.

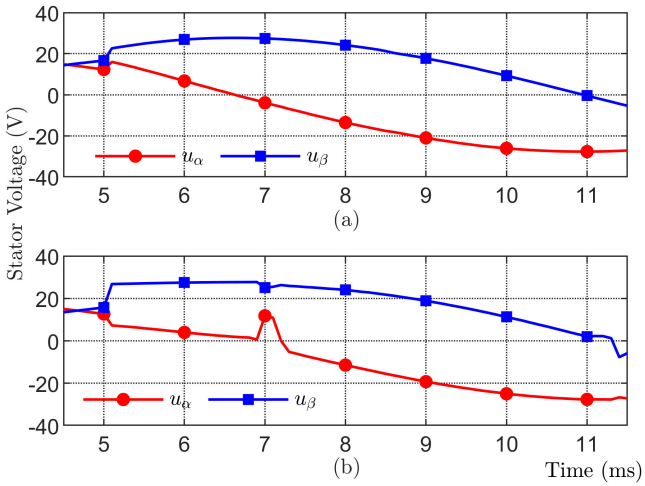

Fig. 7. Simulation results of stator voltage at 800 r/min, current reference is 1.2 A. (a) Classical DPCC. (b) Modified deadbeat predictive current control.

the optimal VV of classical DPCC is in the linear region of SVM, the classical DPCC method can be directly implemented and the motor reaches steady state.

There are three reasons why the proposed method was designed to be combined with classical DPCC. First, the deadbeat method shows better dynamic and steady-state performance than classical simple methods, such as PI-SVM. Also, classical methods such as PI requires parameters tuning, while the deadbeat method is based on the motor model with no other parameter tuning. In addition, deadbeat control methods have many advantages, such as lower computation complexity than methods based on FCS-MPC, and it was simple and stable to be combined with the proposed M-DPCC together.

A. Simulations

Comparative simulation results are carried out in Figs. 4 –7. In Figs. 4 and 5, the SPM was set at constant speed of 600 r/min with no load in initial state. A step current of 2.3 A is applied to the motor at 5 ms. The current dynamic response using classical DPCC is shown in Fig. 4(a). Note that only the sampled current at each control cycle is plotted on the figure and the current ripples between sample points are ignored. The q-axis current error was eliminated at 10 ms, which means the current transient state consisted of 40 control cycles. During the dynamic interval, the d-axis current was regulated to maintain zero. After the dynamic interval, the motor entered steady state and MTPA, i.e., id $= 0$ control strategy of SPM was implemented.

The current dynamics of the proposed M-DPCC is shown in Fig. 4(b). Compared to classical DPCC, the d-axis current had a flux-weakening component during the dynamic interval, which improve the dynamic performance of the q-axis current. The q-axis current error was eliminated in 30 control cycles, which is 25% faster than classical DPCC. The VV in $\alpha\beta$-axis in the dynamic interval is shown in Fig. 5. For classical DPCC, when faced with current reference variation at 5ms, the VV

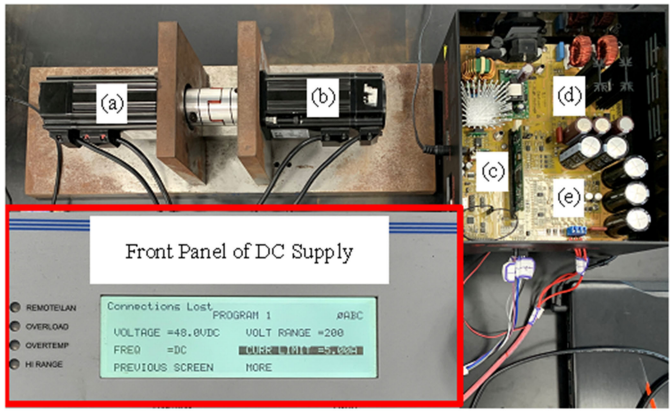

Fig. 8. Experiment rig. (a) Load motor. (b) Test motor. (c) DSP TMS320-F28335. (d) DC supply input. (e) Inverter.

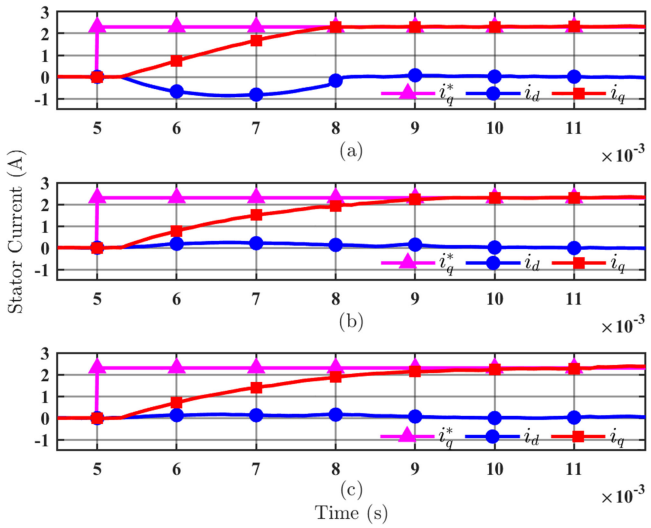

Fig. 9. Experimental results of current dynamic performance at 600 r/min, load current reference is 2.3 A. (a) Modified deadbeat predictive current control. (b) Deadbeat predictive current control. (c) Modulated model predictive control.

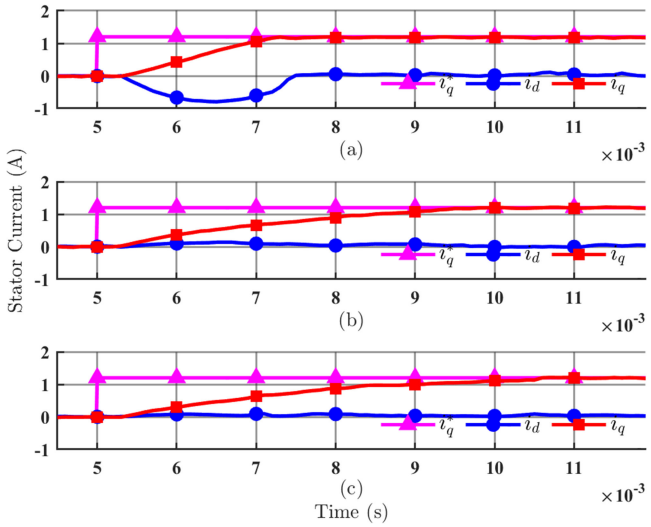

Fig. 10. Experimental results of current dynamic performance at 800 r/min, load current reference is 1.2 A. (a) Modified deadbeat predictive current control. (b) Deadbeat predictive current control. (c) Modulated model predictive control.

of classical DPCC must be limited in the SVM linear region. Hence, only the amplitude of VV increases while the angle maintains, as explained in (8). For M-DPCC, when faced with limitation, the angle of VV changed to optimize the torque dynamic performance, which is shown in Fig. 5(b). According to (22), the optimal VV maintains constant in the entire dynamic interval. However, the angle of the optimal VV slightly changed during the interval due to the small rise in the rotor speed. Another simulation of current response is shown in Figs. 6 and 7. The motor was at 800 r/min and no load in the initial state. A step current of 1.2 A is applied to the motor at 5ms.

Comparison of the q-axis current dynamic performance between the classical DPCC and M-DPCC indicates that at this operating point, M-DPCC improves the torque dynamic performance by 33%. Both simulations reflect that M-DPCC shows good torque dynamic improvement of the tested SPM around rated speed and rated load.

B. Experimental Results

The performance of the proposed M-DPCC, classical DPCC and MMPC in [36] are investigated experimentally. The experimental setup is shown in Fig. 8. The system consists of the load motor, the test SPM motor and the converter with TMS320F28335 digital signal processor (DSP). The nominal parameters of both motors are the same as given in Table I. Parameter sensitivity is a big issue for DPCC methods. The stator inductance is sensitive to stator saturation which is caused by stator currents. It is most variable and may cause reduction of steady- and transient-state performance. However, the motor in the experiment is a servo motor. One the one hand, the rated condition of servo motors on B–H curve is usually set lower to avoid too much saturation to maintain control performance. Hence, the variations of the parameters between no-load and rated-load in our case is small. One the other hand, the same parameter given in Table I will be used in the proposed M-DPCC and tested in a wide working range including maximum current condition to ensure the robustness of the proposed method. In addition to that, the comparative experimental results of the three methods under motor inductance variation between -50% to +100% are also carried out to verify the robustness of the proposed method to motor inductance variation.

1) Dynamic Performance: Comparative experiments of classical DPCC, M-DPCC, and MMPC in the transient state are shown in Figs. 9 and 10. In Fig. 9, the load motor kept the constant speed of 600 r/min and then the load current of 2.3 A was applied to the test motor at 5 ms. For classical DPCC and MPCC, the q-axis current reaches its reference at 9 ms, and the d-axis current remained close to zero during the dynamic interval. For the proposed M-DPCC, the q-axis current reached its reference at 8 ms, which is 25% faster than both classical DPCC and MMPC.

The dynamic response of the proposed M-DPCC is shown in Fig. 9(a). There was inter-coupling between the d-axis and

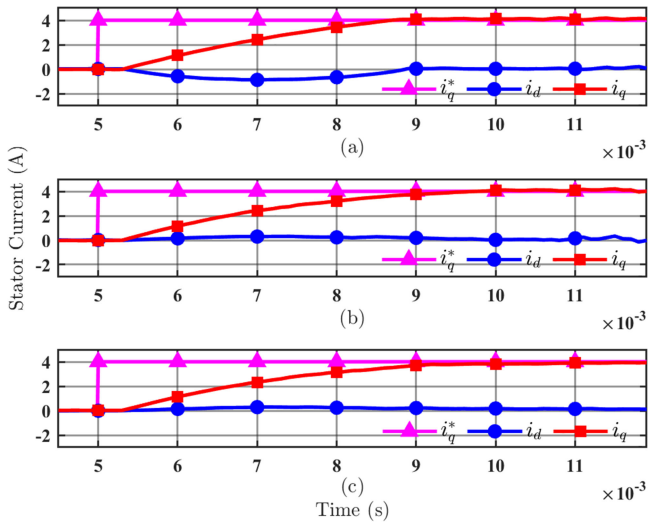

Fig. 11. Experimental results of current dynamic performance at 400 r/min, load current reference is 4 A. (a) Modified deadbeat predictive current control. (b) Deadbeat predictive current control. (c) Modulated model predictive control.

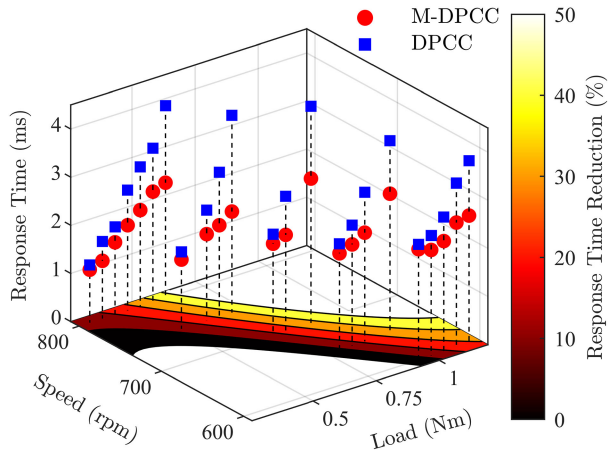

Fig. 12. Torque dynamic performance comparison in rated operation area.

q-axis current, as the flux-weakening current component was introduced during the interval. It improved the dynamic performance of q-axis current. As the intercoupling decreases the torque per ampere ratio in the steady state, the d-axis current was eliminated in the steady state. Hence, in the steady state, there was no intercoupling between the d-axis and q-axis current. Because the intercoupling only occurred in the transient state, the copper loss and efficiency loss can be ignored. MTPA can be achieved in the steady state to reduce copper loss and improve motor efficiency.

Similarly, the test motor was operated at 800 r/min, as shown in Fig. 10. The M-DPCC achieved 50% improvement of q-axis current response compared with classical DPCC and MMPC.

For the lower speed and largest load, M-DPCC, classical DPCC and MMPC performance have similar dynamic performance, Fig. 11 . MPCC reached q-axis current reference at 9.5 ms while classical DPCC and M-DPCC reached reference at 10 ms.

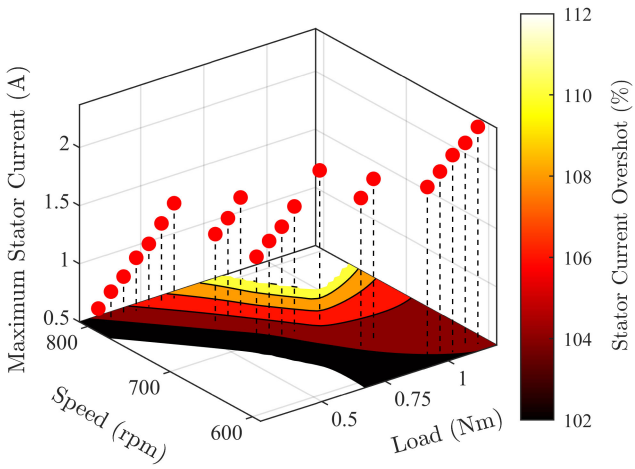

Fig. 13. Current vector amplitude overshot of M-DPCC in rated operation area.

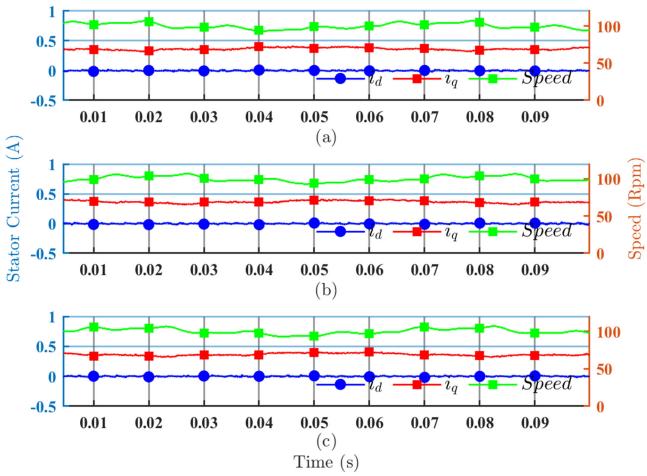

Fig. 14. Steady-state performance at 100 r/min without load, from DSP data. (a) Modified deadbeat predictive current control. (b) Deadbeat predictive current control. (c) Modulated model predictive control.

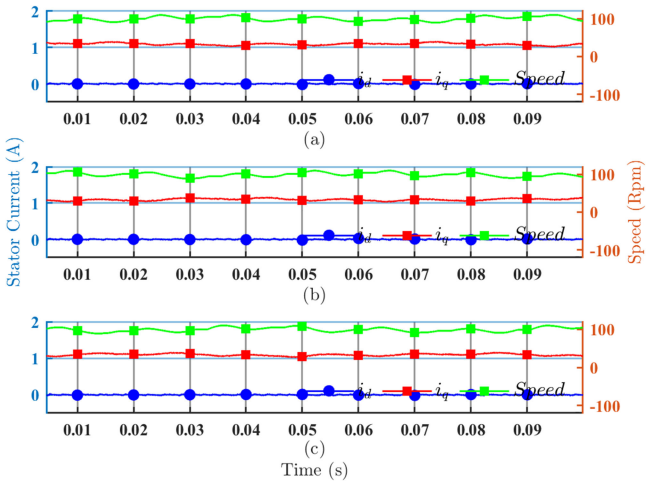

Fig. 15. Steady-state performance at 100 r/min with 1 A load current, from DSP data. (a) Modified deadbeat predictive current control. (b) Deadbeat predictive current control. (c) Modulated model predictive control.

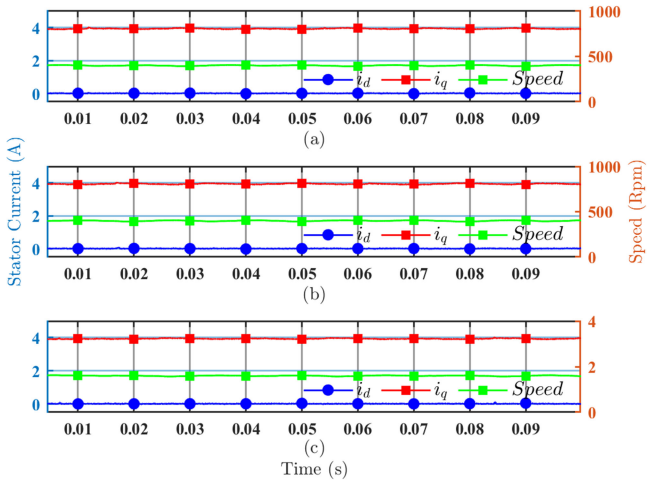

Fig. 16. Steady-state performance at 400 r/min with largest 4 A load current, from DSP data. (a) Modified deadbeat predictive current control. (b) Deadbeat predictive current control. (c) Modulated model predictive control.

A comprehensive investigation of the torque dynamic performance of M-DPCC and classical DPCC are carried out in Fig. 12. Operation conditions between 600–800 r/min and 1–2.3 A are tested to certify the dynamic performance of the proposed M-DPCC and its robustness to motor parameters variations in wide range operations. In rated speed and heavy load operation area, M-DPCC shows linear relation between response time and load, while the dynamic performance of classical DPCC decreases rapidly. Evident dynamic performance improvement up to 50% is achieved using M-DPCC.

The extra d-axis current in the dynamic interval of M-DPCC may cause overshot in the current vector magnitude compared to classical DPCC which maintains the d-axis current to be zero. Hence, no overshot in the current vector magnitude occurs. The amplitude overshot of M-DPCC in rated area is shown in Fig. 13. In rated speed and heavy load area, the current vector amplitude overshot is up to 110%, in low speed and low load area, as the dynamic improvement of M-DPCC decreases the overshot caused by d-axis current decreases at the same time. The overshot happened after the q-axis current error had been eliminated while the d-axis current error had not, and the q-axis current maintained stable during the d-axis current regulation. Therefore, the overshot will not cause torque ripples.

2) Steady-State Performance: All the three method, M-DPCC, classical DPCC and the latest MMPC achieved SVM modulation in the steady state, therefore, the performance of current ripple, torque ripple and current THD are similar. Comparative experiments of the three methods are carried out in this section, in the form of both DSP recorded data and oscilloscope figure.

First, the test motor ran at very low speed without load. As shown in Fig. 14, the proposed M-DPCC, classical DPCC and MMPC performed similarly at low speed and low current reference. Besides, the results of low speed and torque values at 100 r/min, 1 A are carried out in Fig. 15. The current errors and current ripples of the three methods were similar.

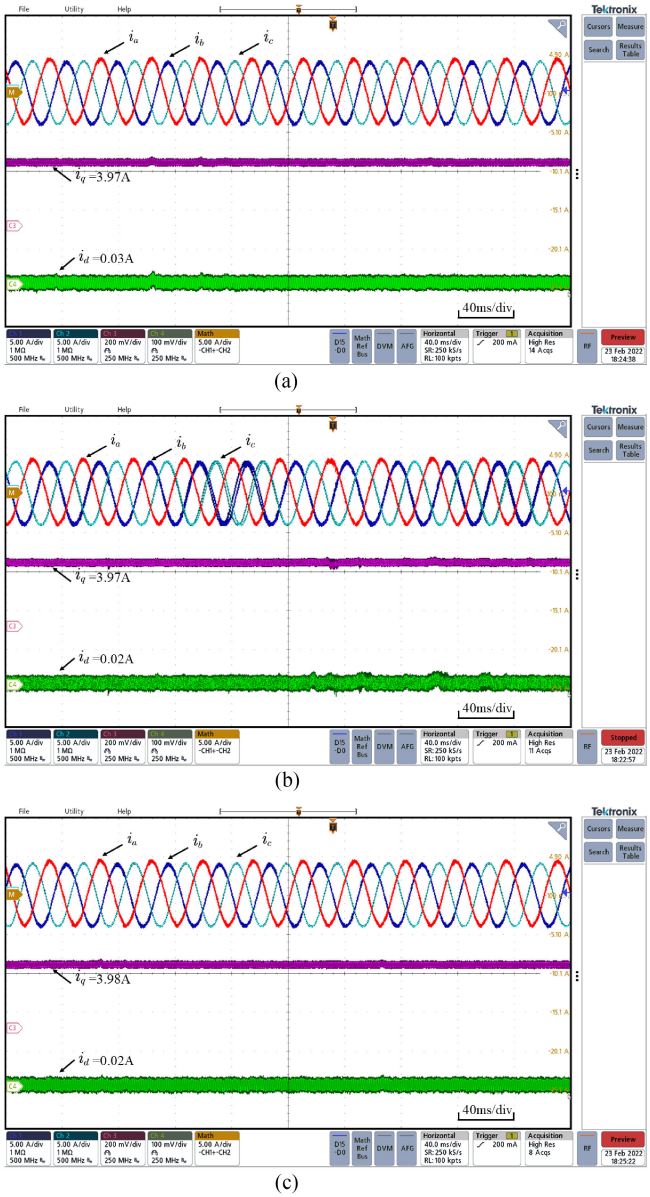

Fig. 17. Steady-state performance at 400 r/min with largest 4 A load current, from oscilloscope capture. (a) Modified deadbeat predictive current control. (b) Deadbeat predictive current control. (c) Modulated model predictive current control.

Another big issue for MPC is parameter variations when working condition changed. Therefore, the largest current of 4 A was added to the test motor under 400 r/min. As shown in Figs. 16 and 17, all three methods performed similar when faced with large current and maximum inductance variation caused by current.

Steady-state performances of the three methods under rated condition were also tested. Motor ran at 600 r/min with 2.3 A rated current. The rated condition performances of the three methods are shown in Fig. 18. The proposed M-DPCC, classical DPCC and MMPC all performed stable in speed ripples and current errors.

To validate the steady-state performance of the three methods, steady-state phase current THD and q-axis current error at

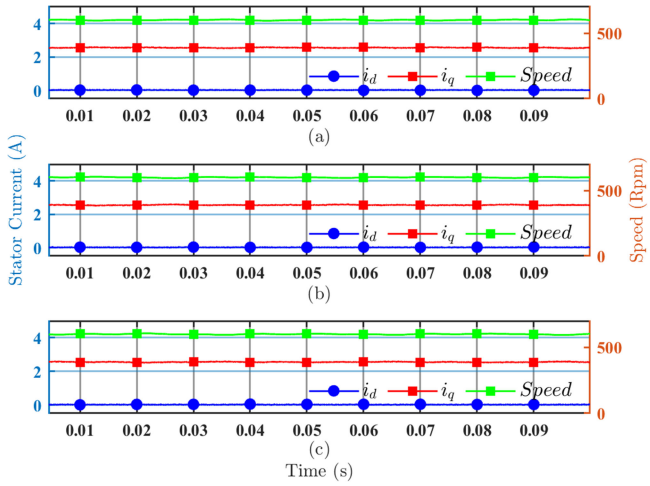

Fig. 18. Steady-state performance at 600 r/min with 2.3A current (rated), from DSP data. (a) Modified deadbeat predictive current control. (b) Deadbeat predictive current control. (c) Modulated model predictive control.

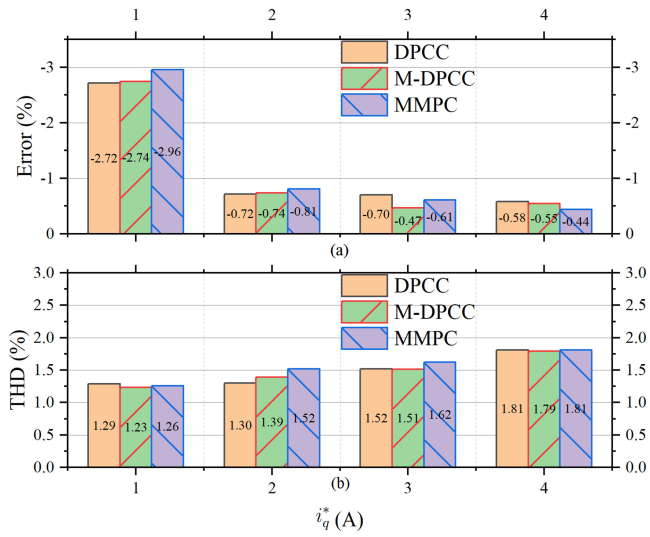

Fig. 19. Steady-state phase current THD and q-axis current error at 400 r/min. (a) q-axis current error. (b) Phase current THD.

400 r/min are acquired by digital power meter YOKOGAWA WT1600. As shown in Fig. 19(b) , the phase current THD of MMPC was higher than M-DPCC and classical DPCC, while the phase current THD of M-DPCC and classical DPCC maintained at the same level. In Fig. 19(a), the q-axis current steady-state error decreased when the current amplitude rose. It is because the PMSM model became less accurate when faced with small current and low duty ratio of PWM modulation. Insulated gate bipolar transistor voltage drop, PWM switching deadband and other reasons caused by the inverter might influence the accuracy of PMSM model. When current reference rose, the steady-state errors of the three methods decreased similarly.

3) Parameter Sensitivity: Parameter sensitivity is another important issue in DPCC methods as the motor parameters have significant influence on predictions and evaluations. The stator

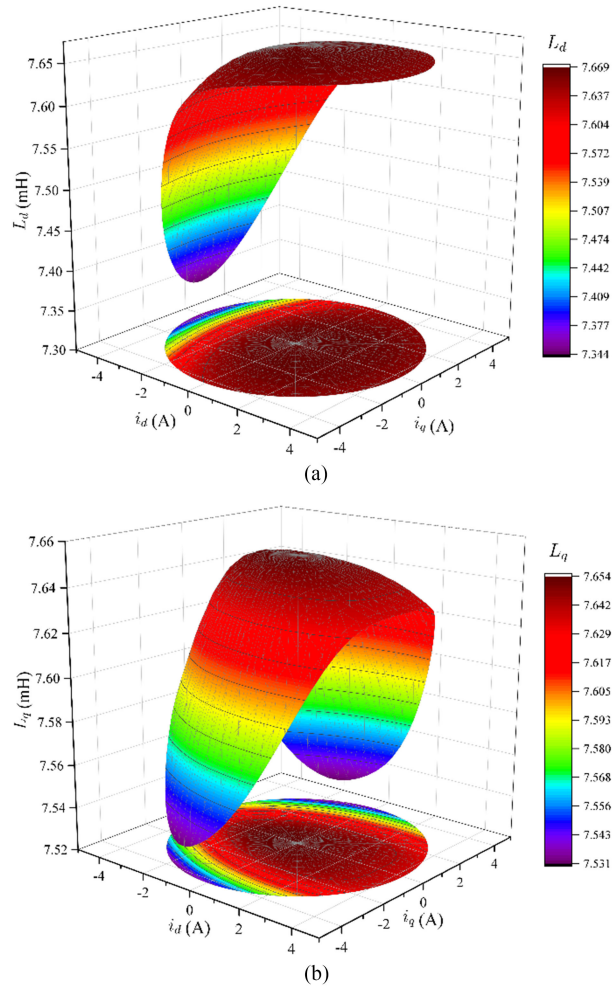

Fig. 20. FE analysis of the test motor. (a) d-axis inductance. (b) q-axis inductance.

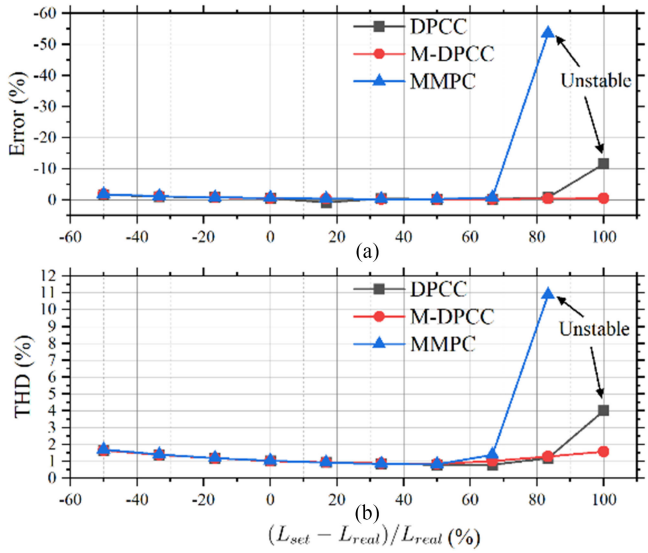

Fig. 21. Experimental Phase current THD and q-axis current error under inductance mismatch. Motor ran at 800 r/min, 0.5 N·m. (a) q-axis current error. (b) Phase current THD.

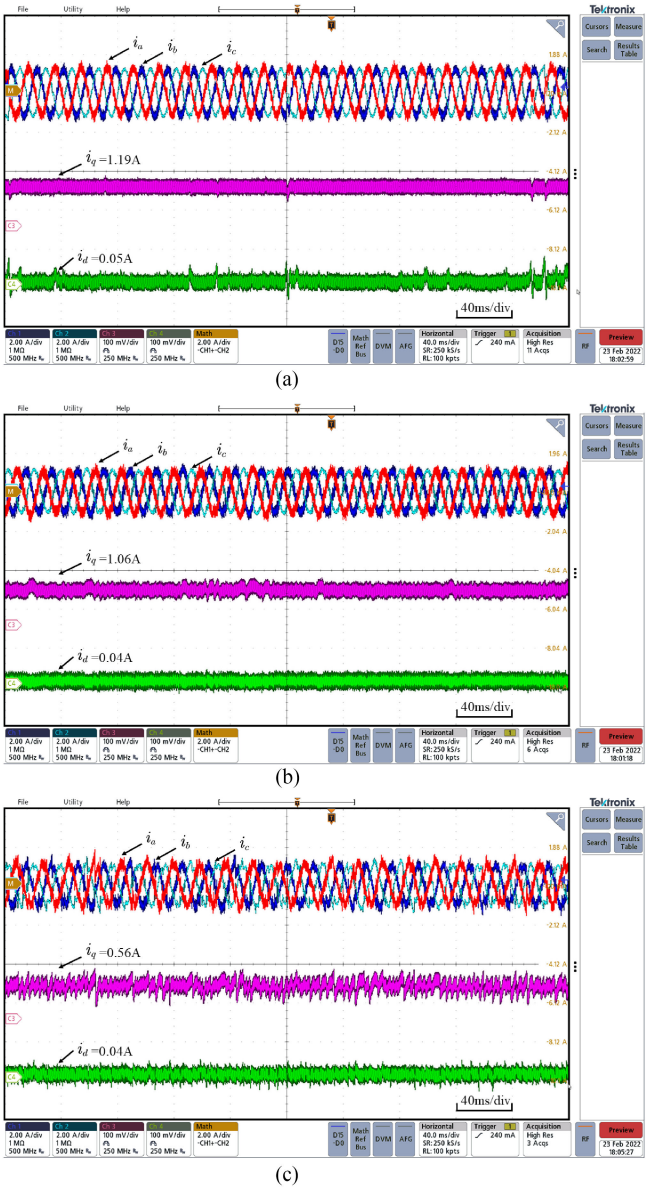

Fig. 22. Steady-state performance under inductance mismatch. Motor ran at 800 r/min with 1.2 A load current, from oscilloscope capture. (a) M-DPCC under +100% mismatch. (b) Classical DPCC under +100% mismatch, (c) MMPC under +80% mismatch.

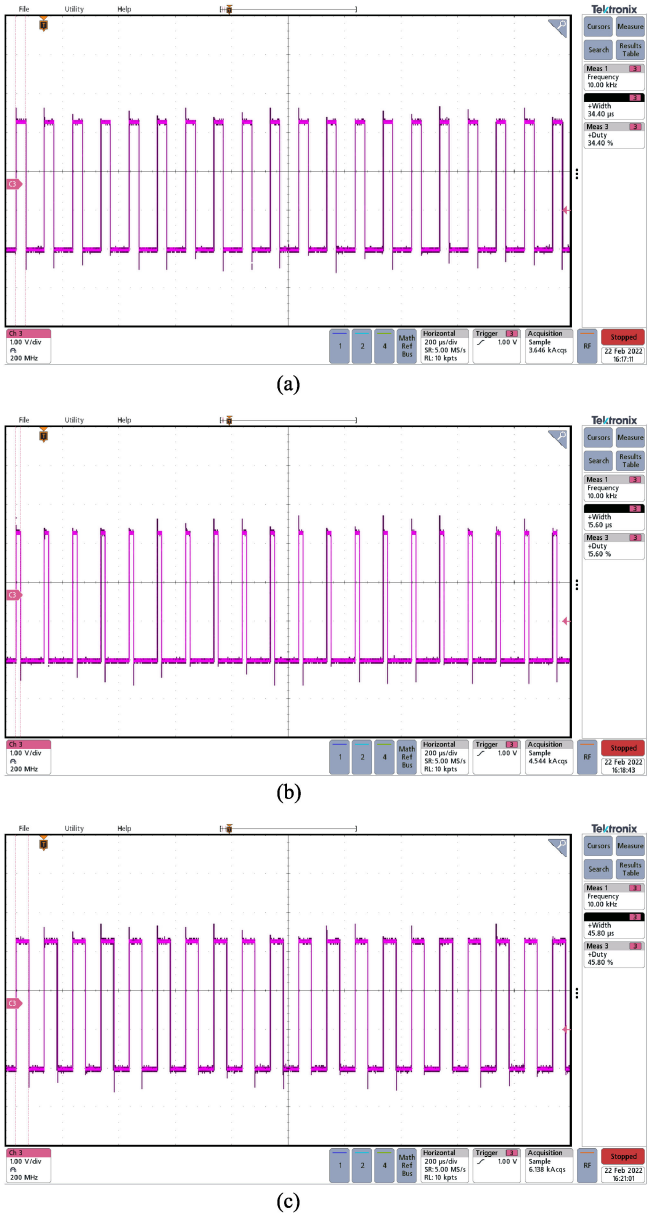

Fig. 23. Computation time of M-DPCC, classical DPCC and MMPC. (a) Modified deadbeat predictive current control. (b) Classical DPCC. (c) Modulated model predictive control.

inductance can be affected by the winding current at different working condition. Therefore, the FE analysis of the test motor based on JMAG were carried out to show the inductance variation, as shown in Fig. 20. The maximum magnetic flux density can reach 1.4T at largest load. Besides, the variations of the d-axis and q-axis inductance in the test motor are less than 4% at different working condition.

Then, the inductance mismatch varying from -50% to +100% was used in the three methods to show their robustness. It was more severe than the FE results. Fig. 21 shows that when the inductance mismatch was within -50% to +70%, all the three methods maintained stable operation. But, when the inductance variation was beyond +70%, the THD and the error of the MMPC increased rapidly and MMPC was out of stable operation range beyond +80% inductance mismatch. When the inductance mismatch was at +100%, classical DPCC was out of stable operation range with increased THD and q-axis current error. However, the proposed M-DPCC maintained stable operation at +100% inductance mismatch. The THD and error were smaller than classical DPCC and MMPC. It indicates that the proposed M-DPCC was more robust than classical DPCC and MMPC in terms of inductance mismatch. Besides, the steady-state current using the three methods with inductance mismatch was captured by oscilloscope, as shown in Fig. 22. The proposed M-DPCC showed lower ripples in d-axis and q-axis current.

4) Computation Complexity: Another important issue is the computation burden of the proposed M-DPCC. Computation time is displayed in Fig. 23. The M-DPCC, classical DPCC and MMPC are run on DSP 28335 and the control frequency is set to be 10 kHz. A general purpose input/output pin is set when the computation started and reset when the computation was over. In comparison, computation duty cycle of the proposed M-DPCC Was 34%, the classical DPCC was 15.6% and the MMPC was 45.8%. the classical DPCC and the MMPC are both single-step MPC methods, but classical DPCC which enabled explicit evaluation had lower computation complexity. The proposed M-DPCC achieved adaptive prediction horizon but the computation complexity is 25% lower than the latest MMPC method.

V. Conclusion

This article proposes a modified DPCC method to improve the dynamic performance of PMSM when there is lack of stator voltage under rated speed and heavy load conditions. The proposed method achieved such improvement by adaptively extending the prediction horizon to the entire dynamic interval. The additional computation burden caused by the extension was optimized and reduced by explicit evaluation. The VV angle of DPCC is then optimized and implemented within the dynamic interval. Such operation produces flux weakening current component only under the transient state and can be eliminated in the steady state. The dynamic performance was proved through comparative experiments with classical DPCC and the latest MMPC methods. When the optimal VV is inside the linear region of SVM, M-DPCC has the same performances as classical DPCC and MMPC. When overmodulation is required, optimal VV can be applied and the dynamic performance can be improved. Also, the proposed M-DPCC was experimentally proved more robust to severe motor inductance variation than the other two methods, in steady-state phase current THD and q-axis current error. The dynamic response of M-DPCC is over 40% faster than the MMPC and classical DPCC in heavy load condition. Besides, the stable operation range under parameter mismatch is 50% larger than the M-DPCC. Furthermore, the computation time of M-DPCC was reduced by 25% compared with MMPC. The proposed method can be further extended to interior PMSMs.

References

[1] F. Morel, X. Lin-Shi, J. Retif, B. Allard, and C. Buttay, "A comparative study of predictive current control schemes for a permanent-magnet synchronous machine drive," *IEEE Trans. Ind. Electron.*, vol. 56, no. 7, pp. 2715–2728, Jul. 2009.

[2] J. Rodriguez et al., "Latest advances of model predictive control in electrical drives—Part I: Basic concepts and advanced strategies," *IEEE Trans. Power Electron.*, vol. 37, no. 4, pp. 3927–3942, Apr. 2022.

[3] J. Rodriguez et al., "Latest advances of model predictive control in electrical drives—Part II: Applications and benchmarking with classical control methods," *IEEE Trans. Power Electron.*, vol. 37, no. 5, pp. 5047–5061, May 2022.

[4] P. Cortes, M. P. Kazmierkowski, R. M. Kennel, D. E. Quevedo, and J. Rodriguez, "Predictive control in power electronics and drives," *IEEE Trans. Ind. Electron.*, vol. 55, no. 12, pp. 4312–4324, Dec. 2008.

[5] P. Karamanakos, T. Geyer, N. Oikonomou, F. D. Kieferndorf, and S. Manias, "Direct model predictive control: A review of strategies that achieve long prediction intervals for power electronics," *IEEE Ind. Electron. Mag.*, vol. 8, no. 1, pp. 32–43, Mar. 2014.

[6] R. Cagienard, P. Grieder, E. C. Kerrigan, and M. Morari, "Move blocking strategies in receding horizon control," in *Proc. 43rd IEEE Conf. Decis. Control*, Dec. 14–17, 2004, vol. 2, pp. 2023–2028.

[7] T. Geyer, G. Papafotiou, and M. Morari, "Model predictive direct torque control—Part i: Concept, algorithm, and analysis," *IEEE Trans. Ind. Electron.*, vol. 56, no. 6, pp. 1894–1905, Jun. 2009.

[8] I. Jlassi and A. J. Marques Cardoso, "Enhanced and computationally efficient model predictive flux and power control of PMSG drives for wind turbine applications," *IEEE Trans. Ind. Electron.*, vol. 68, no. 8, pp. 6574–6583, Aug. 2021, doi: 10.1109/TIE.2020.3005095.

[9] S. G. Petkar, K. Eshwar, and V. K. Thippiripati, "A modified model predictive current control of permanent magnet synchronous motor drive," *IEEE Trans. Ind. Electron.*, vol. 68, no. 2, pp. 1025–1034, Feb. 2021.

[10] W. Chen, S. Zeng, G. Zhang, T. Shi, and C. Xia, "A modified double vectors model predictive torque control of permanent magnet synchronous motor," *IEEE Trans. Power Elecron.*, vol. 34, no. 11, pp. 11419–11428, Nov. 2019.

[11] S. Wang, C. Xia, X. Gu, and W. Chen, "A novel FCS-model predictive control algorithm with duty cycle optimization for surface-mounted PMSM," in *Proc. 7th IET Int. Conf. Power Electron., Mach. Drives*, 2014, pp. 1–6.

[12] Q. Liu and K. Hameyer, "Torque ripple minimization for direct torque control of PMSM with modified FCSMPC," *IEEE Trans. Ind. Appl.*, vol. 52, no. 6, pp. 4855–4864, Nov./Dec. 2016.

[13] X. Li, S. Zhang, C. Zhang, Y. Zhou, and C. Zhang, "An improved deadbeat predictive current control scheme for open-winding permanent magnet synchronous motors drives with disturbance observer," *IEEE Trans. Power Electron.*, vol. 36, no. 4, pp. 4622–4632, Apr. 2020.

[14] X. Li, W. Tian, X. Gao, Q. Yang, and R. Kennel, "A generalized observer-based robust predictive current control strategy for PMSM drive system," *IEEE Trans. Ind. Electron.*, vol. 69, no. 2, pp. 1322–1332, Feb. 2022.

[15] X. Wang, Z. Wang, Z. Xu, W. Wang, B. Wang, and Z. Zou, "Deadbeat predictive current control based fault-tolerant scheme for dual three-phase PMSM drives," *IEEE J. Emerg. Sel. Topics Power Electron.*, vol. 9, no. 2, pp. 1591–1604, Apr. 2021.

[16] M. S. R. Saeed, W. Song, B. Yu, Z. Xie, and X. Feng, "Low-complexity deadbeat model predictive current control for open-winding PMSM drive with zero-sequence current suppression," *IEEE Trans. Transp. Electrific.*, vol. 7, no. 4, pp. 2671–2682, Dec. 2021.

[17] X. Lin, W. Huang, W. Jiang, Y. Zhao, and S. Zhu, "Deadbeat direct torque and flux control for permanent magnet synchronous motor based on stator flux oriented," *IEEE Trans. Power Electron.*, vol. 35, no. 5, pp. 5078–5092, May 2020.

[18] M. Abdelrahem, C. Hackl, Z. Zhang, and R. Kennel, "Robust predictive control for direct-driven surface-mounted permanent-magnet synchronous generators without mechanical sensors," *IEEE Trans. Energy Convers.*, vol. 33, no. 1, pp. 179–189, Mar. 2018.

[19] Y. Wang et al., "Deadbeat model-predictive torque control with discrete space-vector modulation for PMSM drives," *IEEE Trans. Ind. Electron.*, vol. 64, no. 5, pp. 3537–3547, May 2017.

[20] D. Casadei, G. Serra, and K. Tani, "Implementation of a direct control algorithm for induction motors based on discrete space vector modulation," *IEEE Trans. Power Electron.*, vol. 15, no. 4, pp. 769–777, Jul. 2000.

[21] S. Vazquez et al., "Model predictive control with constant switching frequency using a discrete space vector modulation with virtual state vectors," in *Proc. IEEE Int. Conf. Ind. Technol.*, 2009, pp. 1–6.

[22] T. Türker, U. Buyukkeles, and A. F. Bakan, "A robust predictive current controller for PMSM drives," *IEEE Trans. Ind. Electron.*, vol. 63, no. 6, pp. 3906–3914, Jun. 2016.

[23] X. Zhang, B. Hou, and Y. Mei, "Deadbeat predictive current control of permanent-magnet synchronous motors with stator current and disturbance observer," *IEEE Trans. Power Electron.*, vol. 32, no. 5, pp. 3818–3834, May 2017.

[24] X. Yuan, S. Zhang, and C. Zhang, "Enhanced robust deadbeat predictive current control for PMSM drives," *IEEE Access*, vol. 7, pp. 148218–148230, 2019.

[25] Y. Li, Y. Li, and Q. Wang, "Robust predictive current control with parallel compensation terms against multi-parameter mismatches for PMSMs," *IEEE Trans. Energy Convers.*, vol. 35, no. 4, pp. 2222–2230, Dec. 2020.

[26] P. Kakosimos and H. Abu-Rub, "Deadbeat predictive control for PMSM drives with 3-L NPC inverter accounting for saturation effects," *IEEE J. Emerg. Sel. Topics Power Electron.*, vol. 6, no. 4, pp. 1671–1680, Dec. 2018.

[27] D. E. Gaona, H. El Khatib, T. Long, and M. Saur, "Overmodulation strategy for deadbeat-flux and torque control of IPMSM with flux trajectory control in the stationary reference frame," in *Proc. IEEE Energy Convers. Congr. Expo.*, 2020, pp. 6087–6095.

[28] K. Zhou and D. Wang, "Relationship between space-vector modulation and three-phase carrier-based PWM: A comprehensive analysis [three-phase inverters]," *IEEE Trans. Ind. Electron.*, vol. 49, no. 1, pp. 186–196, Feb. 2002.
[29] J. Holtz, W. Lotzkat, and A. Khambadkone, "On continuous control of PWM inverters in the overmodulation range including the six-step mode," in *Proc. Int. Conf. Ind. Electron., Control, Instrum., Automat.*, 1992, vol. 1, pp. 307–312.
[30] D.-C. Lee and G.-M. Lee, "A novel overmodulation technique for space-vector PWM inverters," *IEEE Trans. Power Electron.*, vol. 13, no. 6, pp. 1144–1151, Nov. 1998.
[31] M. E. Zarei, D. Ramírez, M. Prodanovic, and G. M. Arana, "Model predictive control for PMSG-based wind turbines with overmodulation and adjustable dynamic response time," *IEEE Trans. Ind. Electron.*, vol. 69, no. 2, pp. 1573–1585, Feb. 2022.
[32] A. Brosch, O. Wallscheid, and J. Böcker, "Model predictive control of permanent magnet synchronous motors in the overmodulation region including six-step operation," *IEEE Open J. Ind. Appl.*, vol. 2, pp. 47–63, 2021, doi: 10.1109/OJIA.2021.3066105.
[33] Y. Sun, S. Li, X. Fu, W. Dong, M. Ramezani, and B. Balasubramanian, "Approximate dynamic programming vector controllers for operation of IPM motors in linear and overmodulation regions," *IEEE Trans. Transp. Electrific.*, vol. 7, no. 2, pp. 659–670, Jun. 2021.
[34] X. Zhang, K. Yan, and W. Zhang, "Composite vector model predictive control with time-varying control period for PMSM drives," *IEEE Trans. Transp. Electrific.*, vol. 7, no. 3, pp. 1415–1426, Sep. 2021.
[35] C. F. Garcia, C. A. Silva, J. R. Rodriguez, P. Zanchetta, and S. A. Odhano, "Modulated model-predictive control with optimized overmodulation," *IEEE J. Emerg. Sel. Topics Power Electron.*, vol. 7, no. 1, pp. 404–413, Mar. 2019.
[36] A. Sarajian et al., "Overmodulation methods for modulated model predictive control and space vector modulation," *IEEE Trans. Power Electron.*, vol. 36, no. 4, pp. 4549–4559, Apr. 2021.

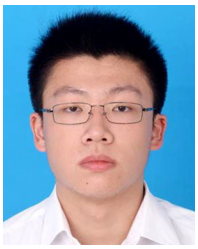

Zixuan Liu was born in Zhejiang Province, China, in 1998. He received the B.Eng. degree in electrical engineering in 2021 from Zhejiang University, Hangzhou, China, where he is currently working toward the Ph.D. degree in electrical engineering.

His research interests include electrical machines and their control systems, and PM machine drives.

Xiaoyan Huang (Member IEEE) received the B.E. degree in control measurement techniques and instrumentation from Zhejiang University, Hangzhou, China, in 2003, and the Ph.D. degree in electrical machines and drives from the University of Nottingham, Nottingham, U.K., in 2008.

From 2008 to 2009, she was a Research Fellow with the University of Nottingham. She is currently a Professor with the College of Electrical Engineering, Zhejiang University, China, where she is working on electrical machines and drives. Her research interests are PM machines and drives for aerospace and traction applications, and generator system for urban networks.

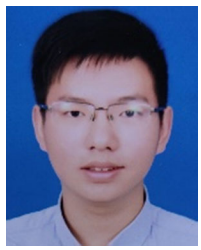

Qichao Hu was born in Zhejiang, China, 1999. He received the B.E. degree in electrical engineering in 2021 from Zhejiang University, Hangzhou, China, where he is currently working toward the M.S. degree in electric machines and electric apparatus.

His research interests include high-performance control methods for servo motors.

Zhaokai Li (Member IEEE) was born in Lishui, China, in 1993. He received the B.S. and Ph.D. degrees in electrical engineering from Zhejiang University, Hangzhou, China, in 2015 and 2020, respectively.

He is currently a Postdoctoral Researcher with Zhejiang University. His major research interests include the analytical modeling of PMSM and iron loss analysis.

Ze Jiang received the Master's degree in 2007 from Zhejiang University, Hangzhou, China, where he is currently toward the Doctorate degree.

Since 2007, he has been engaged in motor and control technology and product development in Wolong Electric Group Co., Ltd. He is currently a Senior Engineer with Zhejiang University. At present, the main research direction is the design and application of high-efficiency PMSM motors and drives systems.

Yelong Yu was born in Zhejiang, China, in 1995. He received the B.Eng. degree in electrical engineering in 2018 from Zhejiang University, Hangzhou, China, where he is currently working toward the Ph.D. degree in electrical engineering. His research interests include the motor drive and control for permanent magnet synchronous motors.

Zhuo Chen was born in Sichuan Province, China, in 1996. He received the B. S. degree in electrical engineering in 2018 from Zhejiang University, Hangzhou, China, where he is currently working toward the Ph.D. degree in electrical machines and drives.

His current research interests include the design of permanent-magnet machines for aerospace and traction applications.